

1 FAST-*forge* – a new cost-effective hybrid processing route for consolidating titanium
2 powder into near net shape forged components

3 N. S. Weston^{*a}, M. Jackson^a

4 ^aThe University of Sheffield, Department of Materials Science and Engineering, Sir Robert Hadfield Building, Mappin
5 Street, Sheffield, S1 3JD, United Kingdom.

6 *Corresponding author email: n.weston@sheffield.ac.uk

7 **Abstract**

8 Reducing the high cost of titanium to a level where it can compete with currently used commodity metals
9 offers opportunities to many industries to exploit its excellent combination of properties to improve
10 performance or reduce weight. The key to decreasing cost is to reduce the number of processing steps to go
11 from ore to component, as well as material wastage from excessive machining. This paper describes a new
12 solid-state hybrid manufacturing route, termed by the authors as FAST-*forge*, for converting titanium alloy
13 powder into components with wrought properties in two steps; utilising field assisted sintering technology
14 (FAST) to produce a shaped preform billet that is finished to near net shape by a one-step precision hot
15 forge. The route has been demonstrated at the laboratory scale using Ti-6Al-4V hydride-dehydride powder
16 by producing fully consolidated, microstructurally homogeneous, double truncated cone specimens directly
17 through FAST, which were then upset forged at a range of temperatures and strain rates. The
18 microstructural evolution and forging behaviour of the Ti-6Al-4V after FAST consolidation is similar to
19 conventional melt, multi-step forged product. Break up of primary α at high strains was observed at 950°C
20 and 0.01 s⁻¹, 0.1 s⁻¹, and 1 s⁻¹. There is good agreement between finite element modelling of the hot forging
21 and the experimental data, which will enable more complex shaped geometries to be produced via the
22 proposed FAST-*forge* route in future. Such a route could be used to consolidate powder from a lower-cost
23 alternative extraction method to become a disruptive technology that will enable a step-change in the
24 economics of titanium components.

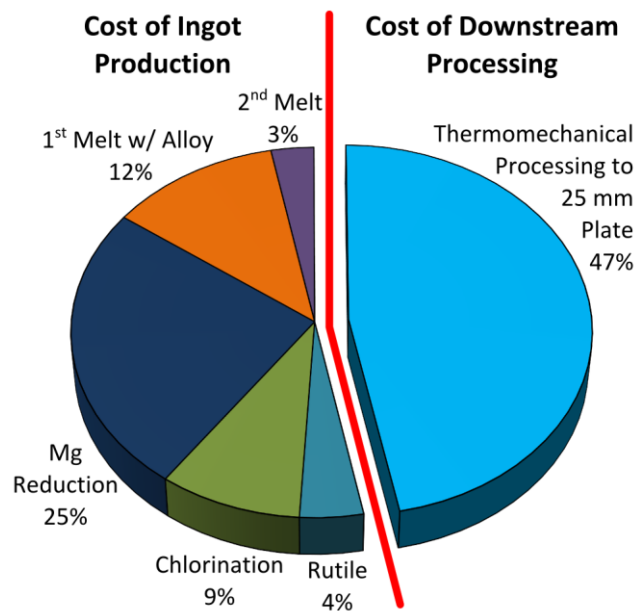
25 *Keywords:* Spark Plasma Sintering (SPS); Pulsed Electric Current Sintering (PECS); Field Assisted Sintering
26 Technology (FAST); Ti-6Al-4V; thermomechanical processing; hot forging.

27 **1. Introduction**

28 Titanium alloys exhibit excellent properties such as a higher specific strength than steels, exceptional
29 corrosion resistance, high melting point and low thermal expansion. Yet titanium's high affinity for
30 embrittling interstitials, such as oxygen, requires inert atmospheres during extraction and downstream
31 processing. Such requirements are reflected in the high cost of titanium mill product and its limited use in
32 non-aerospace sectors. This cost can be approximately broken down into two main areas, which is illustrated
33 by the example of 25 mm thick plate in Fig. 1. The first area is ingot production, accounting for around half of
34 the total cost, which encompasses the ore handling, Kroll process extraction, alloying and melting; most
35 commonly via vacuum arc remelting (VAR), sometimes in combination with electron beam or plasma arc
36 cold hearth remelting. The remaining cost is found in the second area of downstream processing, which in
37 this example is the thermomechanical processing of the VAR ingot; normally multi-stage forging and re-heats
38 to generate the component shape and required properties. As the complexity of the final component
39 increases so does the proportion of the cost from downstream processing due to additional costly steps,
40 such as secondary forging and machining. An approach that targets cost reductions in both areas is required
41 for titanium to compete with commodity metals in non-aerospace sectors. Combining an alternative
42 extraction method with subsequent cost-effective downstream processing offers the potential for significant
43 price decreases.

44 The opportunity presented by a viable lower-cost alternative to the sixty-year-old Kroll process has led to the
45 development of multiple different approaches around the globe; an overview and discussion of a variety of
46 these can be found in (Fray, 2008), with a selection briefly discussed here. In the UK, electro-deoxidation is
47 being developed (Mellor et al., 2015), including the production of novel titanium alloys directly from
48 synthetic rutile feedstock (Benson et al., 2016). Several methods are being investigated in the USA: using
49 hydrogen during the Kroll process' chlorination stage to produce TiH_2 powder, which can then be densified
50 and simultaneously dehydrided by a variety of methods, is reportedly occurring at the pilot-plant scale (Duz
51 et al., 2016); performing nearly continuous sodium reduction of $TiCl_4$ (Armstrong et al., 1999); and

52 electrowinning from carbothermally reduced titanium oxide (Withers, 2015). In South Africa the use of
 53 continuous metallothermic reduction of $TiCl_4$ in molten salt is being trialled (Van Vuuren et al., 2011). In
 54 Australia the use of continuous magnesium reduction of $TiCl_4$ in a fluidised bed reactor process is being
 55 explored (Doblin et al., 2012). All these alternative extraction processes produce a powder or particulate
 56 titanium product. Importantly, as Fig. 1 illustrates, alternative powder extraction routes alone will be
 57 insufficient to achieve the cost reduction necessary for sectors such as the automotive industry. It is the
 58 subsequent consolidation of powder into mill product and near net shape components that will have the
 59 most dominant effect on cost reduction. Cost savings can be made in downstream processing by removing as
 60 many of the traditional multi-stage thermomechanical processing steps as possible.



61
 62 *Fig. 1: Chart demonstrating the two main areas of production costs for 25 mm titanium alloy plate when*
 63 *conventionally processed; with relative cost factors for each sub-area also shown. Produced from data*
 64 *reported in (Kraft, 2004).*

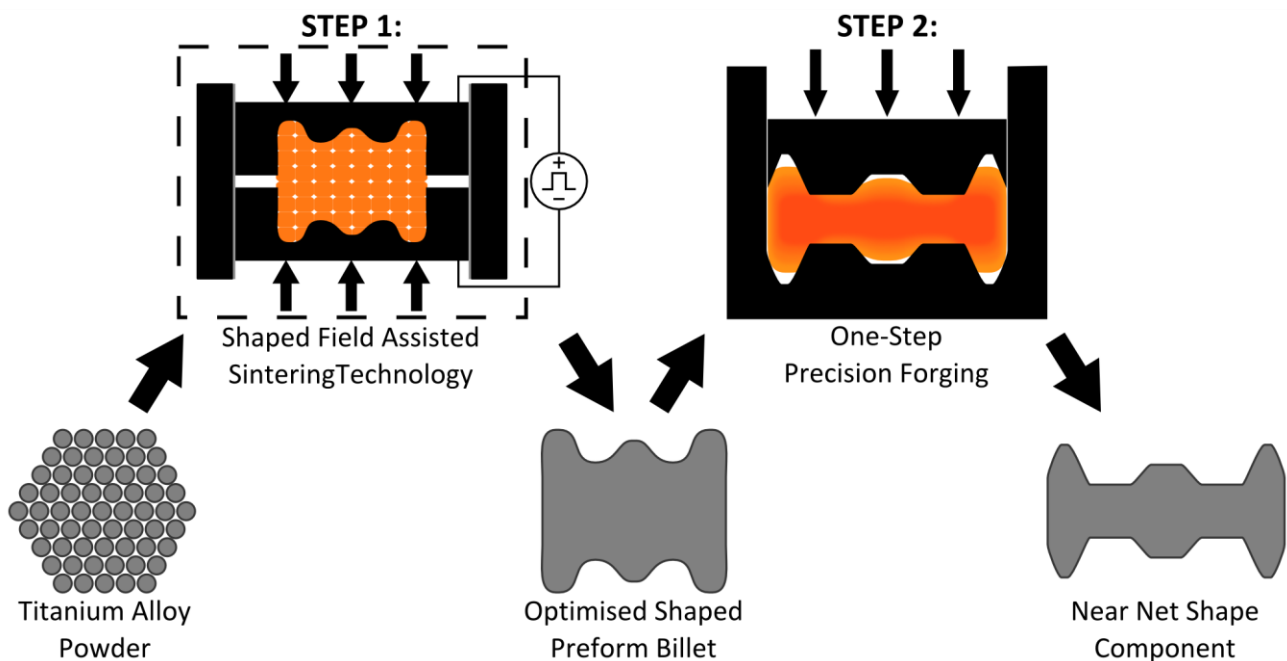
65 Traditional powder metallurgy techniques are able to densify powders without the need for melting, due to
 66 the mechanism of sintering; where adjacent surfaces bond due to diffusional processes that are enhanced by
 67 the application of heat (German, 2014). FAST, also known as spark plasma sintering, allows the solid-state
 68 consolidation of powders by combining the effects of high temperature with the application of uniaxial

69 pressure. The heat is generated through Joule heating as DC current is applied through a mould assembly
70 containing the powder, either continuously or pulsed in a chosen pattern, which allows very high heating
71 rates to be attained compared to more traditional sintering methods. Hydraulically actuated rams allow the
72 application of axial mechanical load to produce the required pressure. FAST is considered an effective
73 method for rapid sintering due to the high heating rates and the blend of heat and pressure; with broad
74 agreement that it can produce equivalent or improved properties, compared with conventional techniques
75 like hot isostatic pressing (HIP), whilst operating with reduced processing times and/or lower temperatures
76 (Munir et al., 2011). This has allowed improved sintering of a range of materials, some that were customarily
77 considered more problematic, such as WC (Orrù et al., 2009). The electric current appears to play a role in
78 enhancing the sintering beyond simple Joule heating, and it is routinely proposed that high localised currents
79 create the eponymous spark plasma, which increases sintering via a mechanism of particle surface cleaning
80 or localised melting/evaporation. However, there is currently insufficient experimental evidence of spark
81 plasma, suggesting that the term is misleading at best; Hulbert et al. were unable to detect it in a variety of
82 powders across a wide spectrum of conditions using a range of techniques (Hulbert et al., 2008). In the
83 absence of spark plasma, other authors have suggested the current might increase diffusion through
84 improving mass transport by electromigration; increased neck growth of copper spheres with increasing
85 current under FAST conditions of fixed temperature, pressure, and time has been shown (Frei et al., 2007). It
86 is clear that complex mechanisms are operating to produce the enhanced sintering that is seen and they are
87 not yet fully understood. From a cost saving perspective FAST may also offer benefits: a 90-95% energy
88 saving has been claimed when using FAST to consolidate $\text{TiAlO}_2 - \text{TiC}$ composites when compared to hot
89 pressing, whilst also reporting a slight improvement in properties (Musa et al., 2009). There is an absence of
90 published work on producing anything other than simple disc shaped specimens via FAST and therefore the
91 limitations of this technology to produce complex geometries is currently unknown.

92 The authors previously indicated the capability of FAST in the sintering of a range of commercial and
93 lower-cost titanium alloy powders (Weston et al., 2015). It was shown that FAST is tolerant of powder
94 morphology and chemistry, and high heating rates could be used to lower processing times with minimal

95 effect on microstructure. Simple disc shapes of constant thickness achieved uniform powder packing and
96 consolidation with no density gradients, which allows microstructural homogeneity throughout specimens,
97 even when scaling up to larger sizes (250 mm diameter and 5 kg); additionally, it was shown that there was
98 limited pick-up (between 100-250 ppm) of carbon, oxygen, and nitrogen from the starting powders. The
99 ability to utilise feedstocks which are larger and angular, including potentially those from alternative
100 extraction methods or even recycled swarf, and still achieve high density and homogeneous microstructures
101 means that FAST has an advantage over traditional sintering operations as these feedstocks are lower-cost.
102 However, the authors believe that the geometries and mechanical properties required by most titanium
103 alloy components will not generally be producible by using FAST as a consolidation process in isolation. The
104 large-grained transformed β microstructure with grain boundary α is not optimal for components that need
105 a good balance of properties; a bi-modal microstructure, produced by hot-working in the α - β phase region,
106 offers advantages for most applications (Lütjering, 1998). The production of complex near net shape
107 geometries directly via FAST may be possible in the future with further investigation although the
108 microstructure would in all likelihood still need refining. Nonetheless, FAST of titanium powder has the
109 potential to be an effective intermediate consolidation and shaping process prior to further
110 thermomechanical processing in the form of a closed-die hot forging operation. To be the most efficient and
111 cost-effective it is possible, with sufficient process design and control, that this could be a one-step near net
112 shape forging operation. To achieve the desired final post-forge geometry and strain levels, and thus
113 microstructures, it is likely that the preform billet produced via FAST will need shape and definition. Finite
114 element (FE) modelling has become a common tool to provide load and microstructural predictions during
115 complex forging operations, although a comprehensive data set is required to achieve this. Therefore, from a
116 process modelling point of view the effect of thermomechanical processing parameters on microstructural
117 evolution needs to be understood due to their inevitable variation, even when nominally isothermal forging.
118 Levels of strain, strain rate and temperature can significantly affect the microstructure of titanium alloys and
119 a large test matrix would be needed to characterise this if using traditional cylindrical axisymmetric
120 compression specimens. The novel double truncated cone testing approach (Jackson et al., 2000) allows this

121 microstructural characterisation in far fewer tests due to the predictable and controlled strain distribution in
122 the forged specimen. A double cone specimen can be tested at a set temperature and strain rate to give
123 information relating to a larger range of strains, from almost zero at the edge to high strains in the centre.
124 Small specimen dimensions can limit temperature variations so that a good approximation of isothermal
125 forging can be realised, as well as allowing metallographic preparation and inspection of the entire
126 specimen.



127

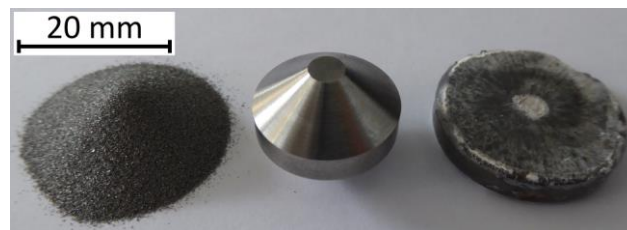
128 *Fig. 2: Schematic diagram outlining the two-step hybrid “FAST-forge” process – a proposed cost-effective*
129 *solid-state processing route for producing titanium alloy components from powder.*

130 The aim of this paper is to demonstrate, at the laboratory scale, that it is possible to produce components
131 from powder in two steps, as shown schematically in Fig. 2; using Field Assisted Sintering Technology (FAST)
132 to produce a shaped preform billet, which is finished to near net shape with one-step precision forging.
133 Depending upon the application it is envisaged that a subsequent heat treatment would allow tailoring of
134 the microstructure if required and/or a minimal finish machining operation would produce an acceptable
135 surface roughness. This novel solid-state hybrid processing route, termed by the authors as “FAST-forge”,
136 will allow manufacturing of components with forged properties for dynamically loaded applications from
137 titanium alloy powders. It is hoped that the mechanical properties achieved by the additional forging of FAST

138 material will allow FAST-*forge* products to be used in areas and applications not conventionally considered
139 possible for as-sintered PM components. It is envisaged that with further development FAST-*forge* will
140 become disruptive technology for a range of sectors. The combination of this cost-effective consolidation
141 method with powder from a lower-cost extraction method will provide a step-change in the economics of
142 titanium components.

143 2. Materials and Methods

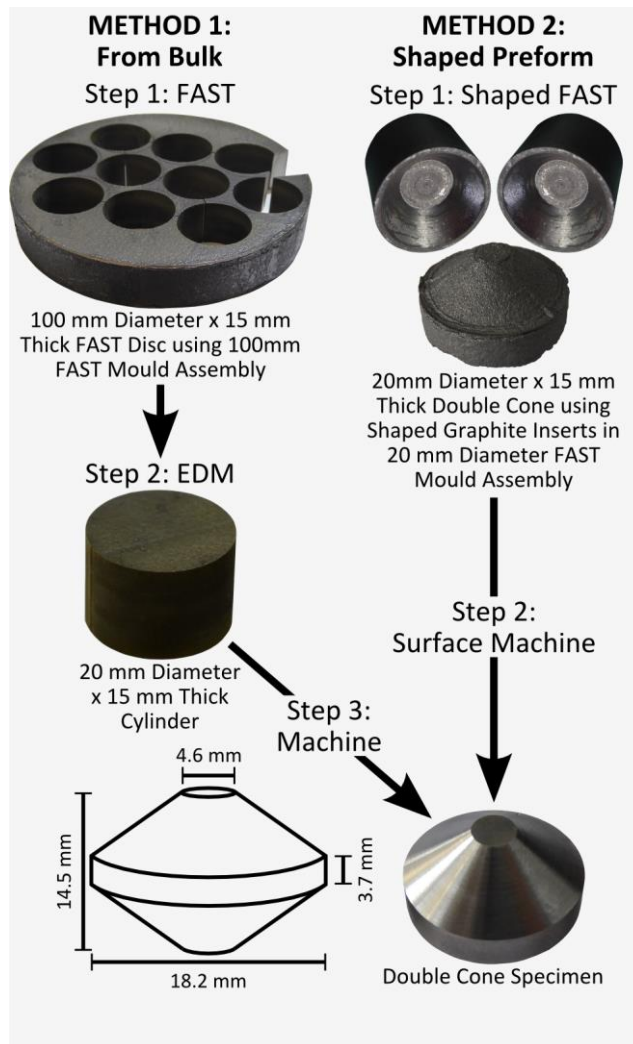
144 2.1 Experimental Approach



145

146 *Fig. 3: Photograph demonstrating the outcome at each stage of the two-step FAST-forge process; the starting*
147 *Ti-6Al-4V HDH powder (left) to the intermediate shaped preform billet, a double truncated cone FAST*
148 *specimen with a light surface machine (centre), and the final forged specimen (right).*

149 The experimental approach aimed to demonstrate three key developments. Firstly, the capability of FAST to
150 produce shaped preforms to be used in the FAST-*forge* process. Secondly that the FAST-*forge* concept, of
151 producing a component with wrought properties from powder in two steps, was viable through a
152 laboratory-scale demonstration, see Fig. 3. Thirdly, to link microstructural evolution of FAST produced
153 preforms to thermomechanical processing parameters by utilising the double truncated cone specimen
154 geometry as the shaped preform billet; thus gaining valuable information for future process optimisation
155 through FE modelling. Ti-6Al-4V hydride-dehydride (HDH) powder was used for this proof of concept
156 demonstration, to enable comparison with conventional wrought product, as well as setting a benchmark for
157 future work with lower-cost powder from an alternative extraction method.



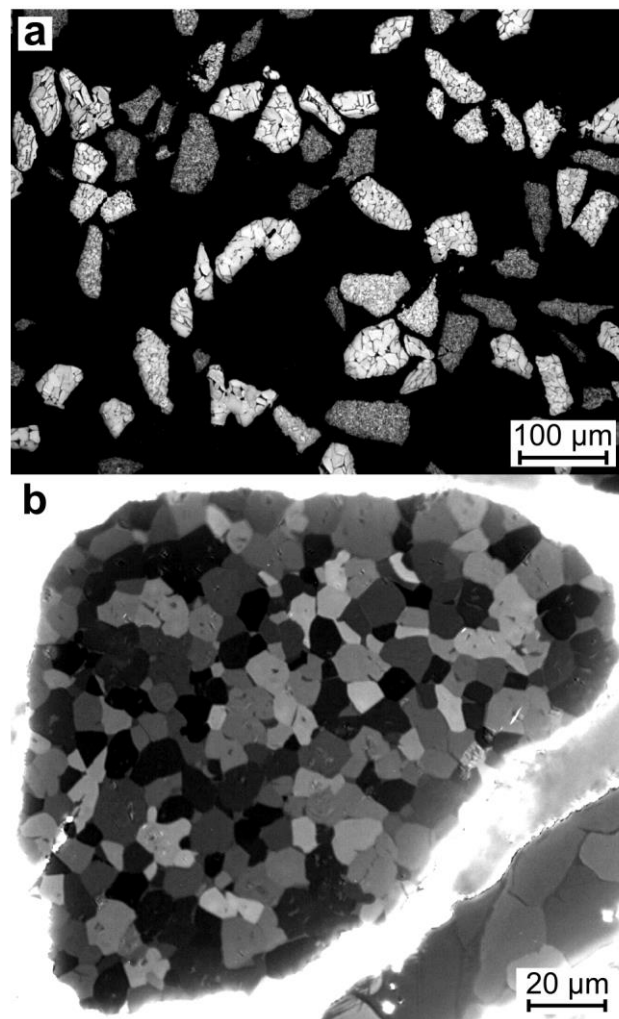
158

159 *Fig. 4: Schematic showing the two methods used to make the double truncated cone specimens. Method 1*
 160 *produced a 100 mm diameter x 15 mm thick FAST disc, which smaller cylinders were extracted from via*
 161 *electro-discharge machining (EDM), and then machined to the final dimensions shown (known as “bulk”*
 162 *double cone specimens). Method 2 used shaped graphite inserts in a 20 mm diameter FAST mould assembly*
 163 *to produce shaped preforms, which then had a surface machine to give the final dimensions shown (known as*
 164 *“shaped” double cone specimens).*

165 Two methods were used to create the double cone specimens, see Fig. 4. The first method was to electrical
 166 discharge machine 20 mm diameter x 15 mm thick cylinders from a 100 mm diameter x 15 mm thick FAST
 167 disc, which were then machined to the final dimensions shown in Fig. 4 (known as “bulk” double cone
 168 specimens hereafter). The second method was to produce shaped preforms by placing shaped graphite
 169 inserts into a 20 mm diameter FAST mould assembly, which were also machined to the same final

170 dimensions (known as “shaped” double cone specimens hereafter). The same sintering cycle and hot
171 compression testing conditions were applied for both methods of double cone specimen production. The
172 aim of creating additional specimens from bulk material was to allow a comparison of behaviour with
173 shaped preform specimens produced directly via FAST; thus demonstrating that the shaped FAST method
174 does not adversely affect either the powder consolidation or subsequent forging response.

175 2.2 Materials



176
177 *Fig. 5: Light micrographs of the Ti-6Al-4V HDH powder's particle morphology after etching with Kroll's*
178 *reagent (a) and microstructure under cross-polarised light (b).*

179 The Ti-6Al-4V HDH powder was purchased from Reading Alloys Inc., (an Ametek Company), Robesonia, PA,
180 USA, and certified to contain 6.34% Al, 4.02% V, 0.21% Fe, 0.026% C, 0.016% H, 0.013% N, and 0.16% O;

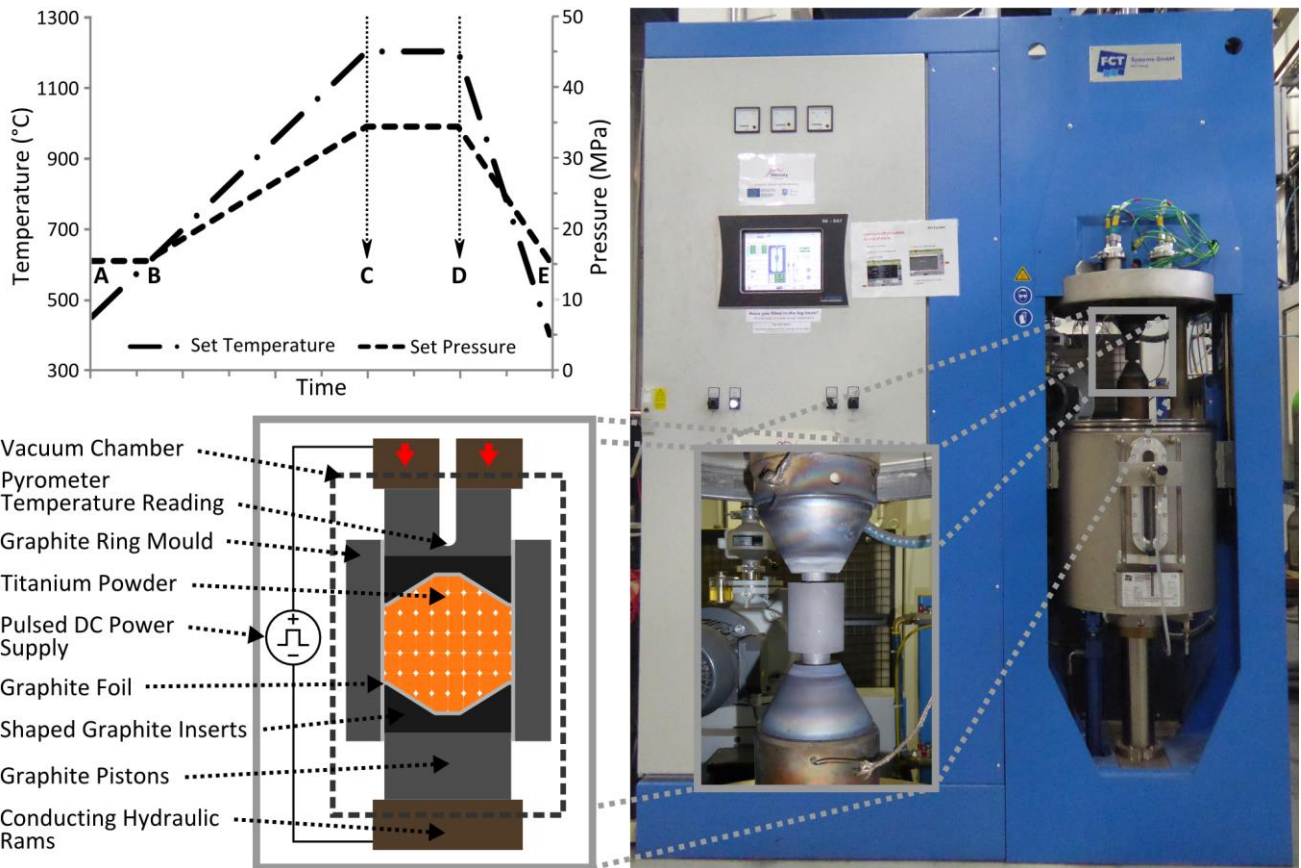
181 therefore meeting the ASTM Grade 5 specification, except 0.001% excess hydrogen. The size range was
182 75-150 μm , with 96.7% of particles within these limits. The powder morphology was angular and irregular in
183 shape, see Fig. 5a, with a microstructure of equiaxed α grains approximately 5-10 μm in diameter, see Fig.
184 5b.

185 **2.3 Methods**

186 2.3.1 Field Assisted Sintering Technology

187 The FAST systems used to consolidate the powder in these experiments were manufactured by FCT Systeme
188 GmbH. The 100 mm disc used for the bulk double cone specimens was made using the Type H-HP D 250
189 system based at Kennametal Manufacturing (UK) Ltd. The shaped double cone specimens were made using
190 The University of Sheffield's Type HP D 25 system, see Fig. 6. The methodology was the same for both
191 machines. The mass of powder required (520 g for bulk and 15 g for shaped) was placed into a graphite ring
192 mould, simply between two graphite pistons for the bulk disc specimen, or with extra shaped graphite
193 inserts for the shaped double cone specimens. Graphite foil was used to line the mould assembly to aid with
194 specimen removal and prolong mould life. The mould assembly was then placed between the two
195 conducting hydraulic rams in the machine's vacuum chamber and held with a put-on load of 5 kN to ensure
196 good electrical contact was made. The sintering cycle used was as follows: the vacuum chamber was
197 evacuated, pulsed DC current was applied in the pattern of 15 ms on and 5 ms off. The values of current and
198 power rose steadily from initial values of 0.45 kA and 2.0 kW to 1.12 - 1.18 kA and 5.9 - 6.3 kW during the
199 dwell period for the shaped double cone specimens. The value of power for the 100 mm disc was a
200 maximum of 163 kW during the heating period and 37 - 42 kW during the dwell period (a sensor fault
201 prevented recording of current data). The heating was uncontrolled up to 450°C due to the operating limits
202 of the pyrometer. Above 450°C a constant heating rate of 100°Cmin⁻¹ was used up to the dwell temperature
203 of 1200°C, points A-C in Fig. 6. Once 600°C was reached, point B, the pressure began to increase, with a rate
204 so that the maximum of 50 MPa would occur simultaneously with the maximum temperature, point C. A
205 dwell time of 30 minutes at maximum conditions was then used, points C-D. For the 100 mm bulk disc the

206 current was then turned off and the specimen allowed to “free” cool, points D-E. For the shaped double
 207 cone specimens, the current was used to achieve a “controlled” cooling rate to match the bulk disc cycle.
 208 The “controlled” cool is achieved by the FAST furnace software reducing the applied current to a level where
 209 the heat loss exceeds the Joule heat generated by the correct amount to attain the desired cooling rate. The
 210 pressure was also gradually decreased back to 5 kN during the cool.

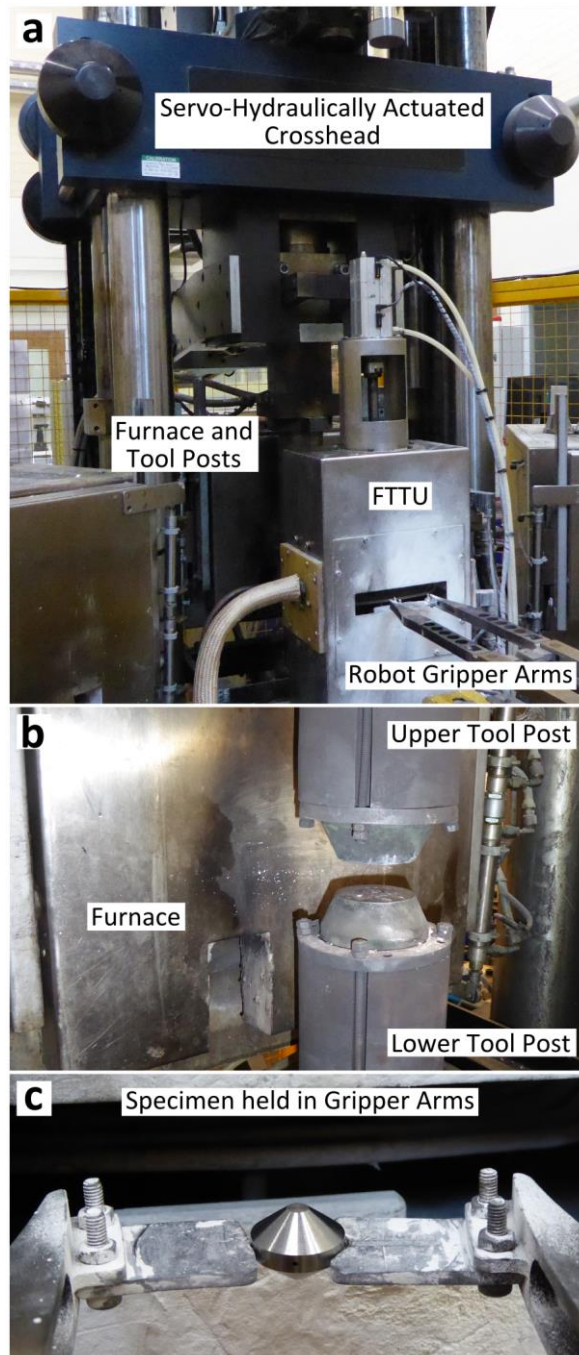


211
 212 *Fig. 6: Photograph of the FCT System GmbH Type HP D 25 FAST Furnace at The University of Sheffield (right);*
 213 *showing detail of the graphite mould assembly held between the conducting hydraulic rams (inset right).*
 214 *Schematic cross-section showing the main components of the FAST system and mould assembly used (bottom*
 215 *left) and a graph outlining the variation in major processing parameters during a typical FAST cycle (top left).*

216 2.3.2 One-Step Forging

217 The replication of the one-step forging stage was undertaken using The University of Sheffield’s
 218 thermomechanical compression testing machine, see Fig. 7. The test furnace contained two M22 steel tool

219 posts, where the upper one was servo-hydraulically actuated, allowing a constant strain rate deformation to
220 a strain of 1.15. A fast thermal treatment unit (FTTU), located immediately in front of the test furnace,
221 allowed induction heating of the double cone specimens at 4°Cs^{-1} to the test temperature, with a hold of 30
222 seconds to minimise any oscillation.



223

224

225

Fig. 7: Photographs outlining the major components of The University of Sheffield's thermomechanical compression machine (a), close-up view of the tool posts and furnace (b) (note the furnace has been moved

226 *to the rear to enable viewing of the tool posts), close-up of a double truncated cone specimen held in the*
227 *robot gripper arms (c).*

228 Robot gripper arms were used to manipulate the specimen during testing; allowing positioning at the correct
229 height before automatically moving into the FTTU and then into the test furnace for the one-step forge,
230 followed by specimen withdrawal for a water quench. A 1.1 mm hole located centrally in the edge of the
231 double cone specimens allowed an N-type thermocouple to be attached; giving control during induction
232 heating and temperature data during deformation. A boron nitride coating was applied to limit interstitial
233 pick up and reduce friction. A data logger recorded time, temperature, load, velocity, and displacement
234 information throughout the test. Bulk double cone specimens were deformed at 850°C, 950°C, and 1050°C,
235 and at strain rates of 0.01 s⁻¹, 0.1 s⁻¹ and 1 s⁻¹. The shaped double cone specimens were deformed at 950°C,
236 at strain rates of 0.01 s⁻¹, 0.1 s⁻¹ and 1 s⁻¹.

237 2.3.3 Finite Element Simulation of the One-Step Forge

238 The finite element software DEFORMTM (Scientific Forming Technologies Corporation, 2016) was used to
239 simulate the compression tests of the double cone specimens to give the strain profiles across the specimens
240 seen in Fig. 11a-11c. These strain profiles allow the linking of microstructural evolution to thermomechanical
241 processing parameters (strain, strain rate, temperature). Due to the axisymmetric nature of the specimens it
242 was possible to use a 2-D model of half the double cone geometry, meshed with 3160 elements, which
243 simplified the simulation and reduced processing time. Rheology data from previous unpublished work, in a
244 tabular form (stress values at a range of strains for each testing condition), was used for the material model,
245 see Table 1 in the appendix. The material response was assumed to be fully plastic. For each test condition
246 the initial temperature was set to that recorded by the thermocouple at the start of the experimental
247 compression, and the measured temperature profile during the tests was used as a boundary condition for
248 the specimen ensuring the simulation matched the experimental conditions as closely as possible. Two
249 non-meshed rigid platens were used to represent the tool posts as their experimental deformation can be
250 treated as negligible. The movement of the upper platen was controlled by setting a condition to produce a

251 constant global average strain rate to match the experiment; the software determined the magnitude of
252 displacement necessary to achieve the set strain rate for each time step. Contact boundary conditions
253 between the specimen and platens were established with a constant shear friction factor (\bar{m}) of 0.3.

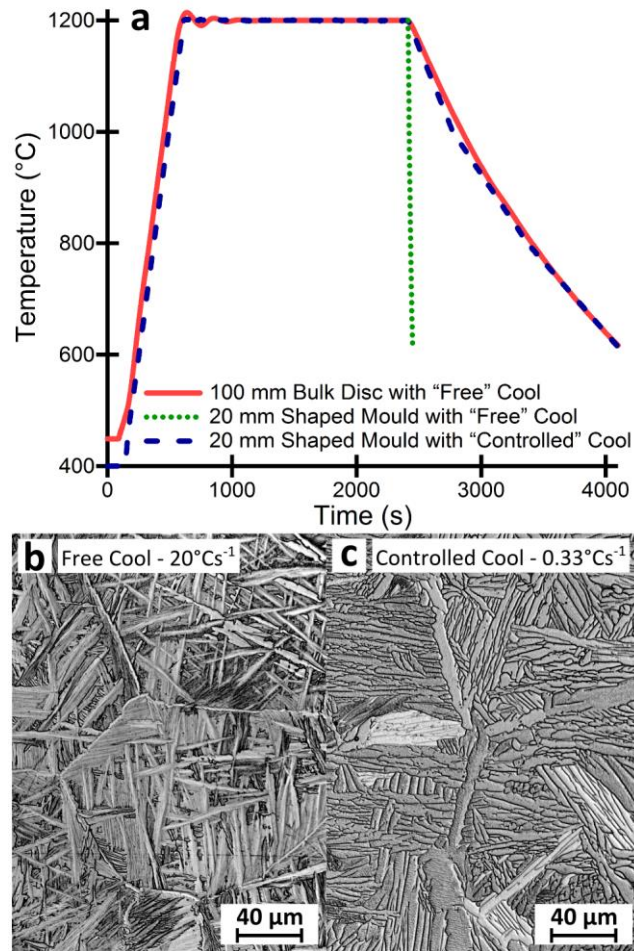
254 2.3.4 Metallography

255 Typical metallographic preparation for Ti-6Al-4V was used for all specimens: sectioned in half parallel to the
256 compression direction, hot-mounted in Bakelite, followed by grinding using progressively finer SiC papers
257 then 9 μm diamond suspension, and finally chemical/mechanical polishing using colloidal silica of 0.05 μm
258 with 20% hydrogen peroxide. Microstructural observations were performed using a Nikon Eclipse LV150 light
259 microscope under reflected light conditions, either in bright field or polarised light mode. Kroll's reagent was
260 applied as an etchant, if needed, until increased microstructural detail was visible.

261 3. Results and Discussions

262 3.1 Microstructures after FAST

263 Preliminary experiments demonstrated that the initial cooling rate after the current is turned off was
264 significantly higher for the 20 mm diameter mould assembly at $\sim 20\text{ }^\circ\text{Cs}^{-1}$ than for the 100 mm diameter
265 mould at $\sim 0.33\text{ }^\circ\text{Cs}^{-1}$, see Fig. 8a. There is greater thermal mass for the larger mould assembly due to the
266 increased amount of graphite required and it therefore takes longer to cool. This work sought to emulate the
267 bulk material as closely as possible to allow direct comparison and therefore a "controlled" cool to match
268 the "free" cool of the bulk was utilised for the shaped double cone specimen. The difference in
269 microstructure produced by free and controlled cool can be seen in Fig. 8b and 8c; as expected the quicker
270 free cool produced much finer α laths, where the controlled slower cool coarsened them to a size similar to
271 the bulk specimen (directly compared in Fig. 9.)



272

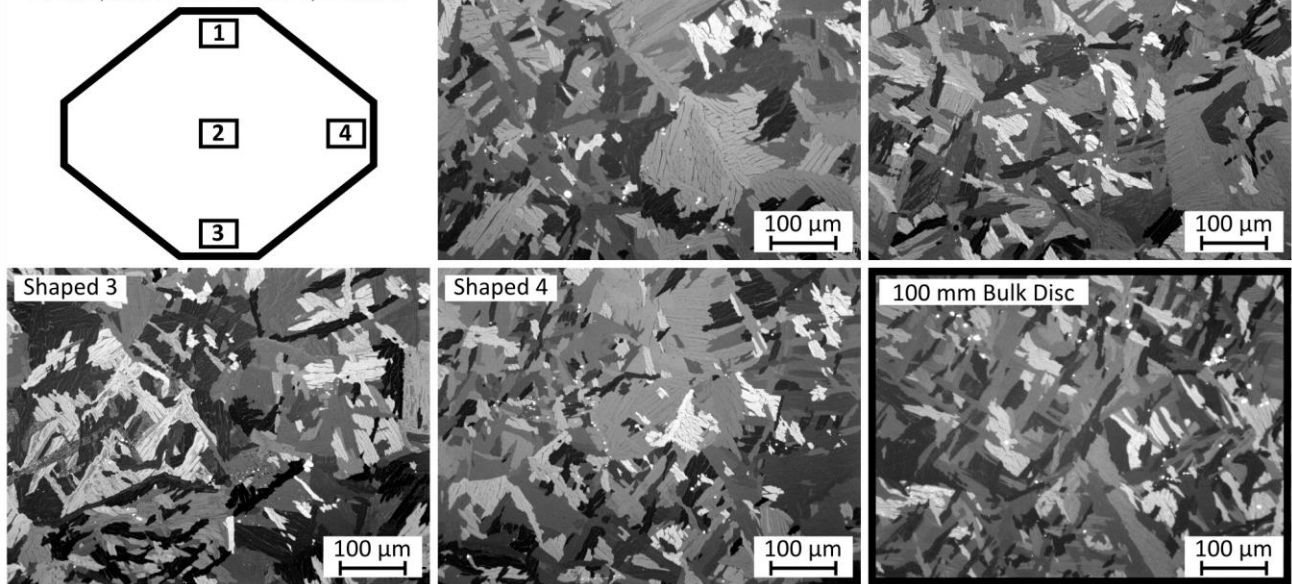
273 *Fig. 8: Graph showing the temperature profiles during FAST processing of three types of Ti-6Al-4V specimen*
 274 *(a). A 100 mm diameter disc used for bulk double cone specimens; allowed to “free” cool after current switch-*
 275 *off (solid line). A 20 mm shaped mould when allowed to “free” cool after current switch-off (dotted line) with*
 276 *associated microstructure (b). A 20 mm shaped mould with “controlled” cool (dashed line) and associated*
 277 *microstructure (c).*

278 The microstructures produced in this work when consolidating the Ti-6Al-4V HDH powder using FAST at a
 279 heating rate of $100^{\circ}\text{Cmin}^{-1}$ with dwell conditions of 1200°C and 50 MPa held for 30 minutes are shown in Fig.
 280 9. A typical microstructure of the 100 mm diameter disc used to produce the bulk double cone specimens is
 281 shown, as are micrographs from selected locations throughout the shaped double cone specimens. Both
 282 specimen types show the expected transformed β microstructure that is characteristically found when slow
 283 cooling from above the β transus temperature; prior β grains containing α laths in a Widmanstätten or

284 colony structure with some amount of α phase present on the grain boundaries (Joshi, 2006). The prior β
285 grain size ranges from approximately 200-600 μm with an α lath width in the region of 3-10 μm . The high
286 temperature and level of consolidation during the dwell period allowed β grain growth beyond the
287 dimensions of the initial powder particles for both bulk and shaped specimens, which is a significant change
288 in microstructure from the starting powder. This β grain growth demonstrates the high density achieved as
289 at lower levels of consolidation the remaining porosity acts to pin grain boundaries and prevent growth.
290 Image analysis, using the software ImageJ (Rasband, 1997), of multiple bright-field micrographs across each
291 specimen allowed the calculation of density as 99.88% for the shaped double cone specimens and as 99.87%
292 for the bulk double cone specimens. These values are slightly greater than the 99.01% stated by (Xu et al.,
293 2014) and slightly less than the 99.9% reported by (Kim et al., 2014) for HIP of Ti-6Al-4V powders, which
294 claimed to have tensile strength and elongation comparable to wrought material. The porosity will also be
295 healed further during the forging process, which will further increase tensile properties and more
296 importantly fatigue strength.

297 It can also be seen in Fig. 9 that microstructural homogeneity was achieved in the shaped double cone
298 specimen, with comparable micrographs from top to bottom and from centre to edge. Graphite has a higher
299 electrical resistivity than Ti-6Al-4V and consequently acts as the main heating element in the mould
300 assembly. Thus, it was hypothesised that a shaped mould, with non-uniform graphite thickness in the axial
301 direction, would produce uneven heating as well as a more complex pressure distribution that would lead to
302 microstructural variations; although this is not observed in the shaped double cones at this scale. If
303 temperature variations were present, they were small enough not to have had a significant effect at the
304 processing conditions used for these experiments. Although this may not be the case if a lower processing
305 temperature is required, especially as the β transus temperature is approached, where there will be a
306 reduction in the diffusional rates with increasing α content. It should be noted that the shape used here is
307 still a relatively simple axisymmetric profile and that further experimentation will be needed, with the aid of
308 FE modelling, to fully understand the difficulties involved in producing semi-complex shaped preform billets
309 as part of the FAST-*forge* processing route.

Micrograph Locations on Cross-Section of Shaped Double Cone Specimen



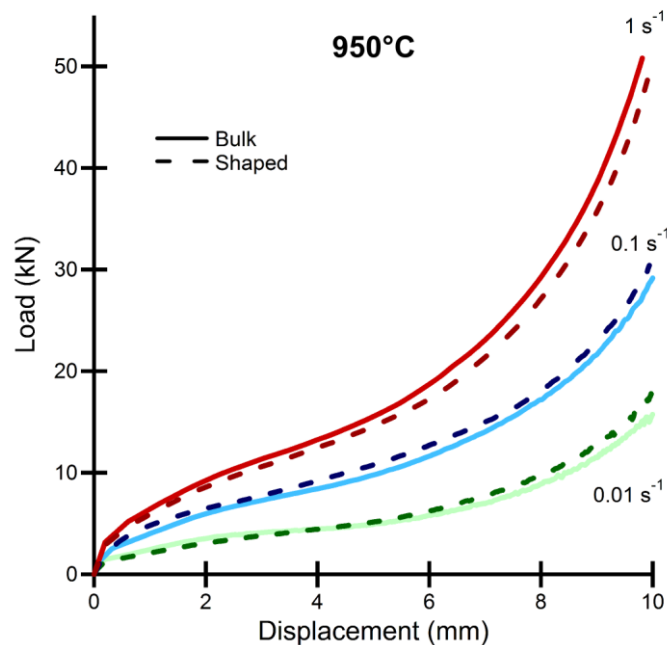
310

311 *Fig. 9: Micrographs of Ti-6Al-4V double truncated cone specimens produced via FAST at a dwell temperature*
312 *of 1200°C. Showing microstructures from a shaped specimen (Shaped 1-4) at the locations outlined in the top*
313 *left diagram; and a characteristic microstructure of the homogeneous bulk specimen (bottom right).*

314 3.2 Experimental Load-Displacement Curves

315 Due to the non-uniform cross-sectional area of the double cone specimens it is not possible to produce
316 meaningful plots of stress versus strain during the thermomechanical compression. Consequently, the data
317 is presented as plots of load versus displacement, which can be seen in Fig. 10 for deformations at 950°C and
318 a range of strain rates. The effect of strain rate is clearly demonstrated; as the rate of deformation increases
319 so does the force required to achieve equivalent displacement. The influence of temperature can be seen in
320 the load-displacement curves at 850°C, 950°C, and 1050°C, see Fig. 12, where there is a marked reduction in
321 the load required for equivalent displacement as temperature increases due to an increase in the more
322 easily deformed β phase and an increase in dynamic recovery and recrystallisation processes. There are
323 some small variations between the load-displacement behaviour of shaped double cone and bulk double
324 cone specimens; at 1 s^{-1} the bulk specimen required a slightly higher load, at 0.1 s^{-1} the bulk specimen
325 required a slightly lower load, and at 0.01 s^{-1} the bulk specimen required a higher load initially before
326 finishing requiring a lower load. The level of variation seen is minimal and would be expected even when

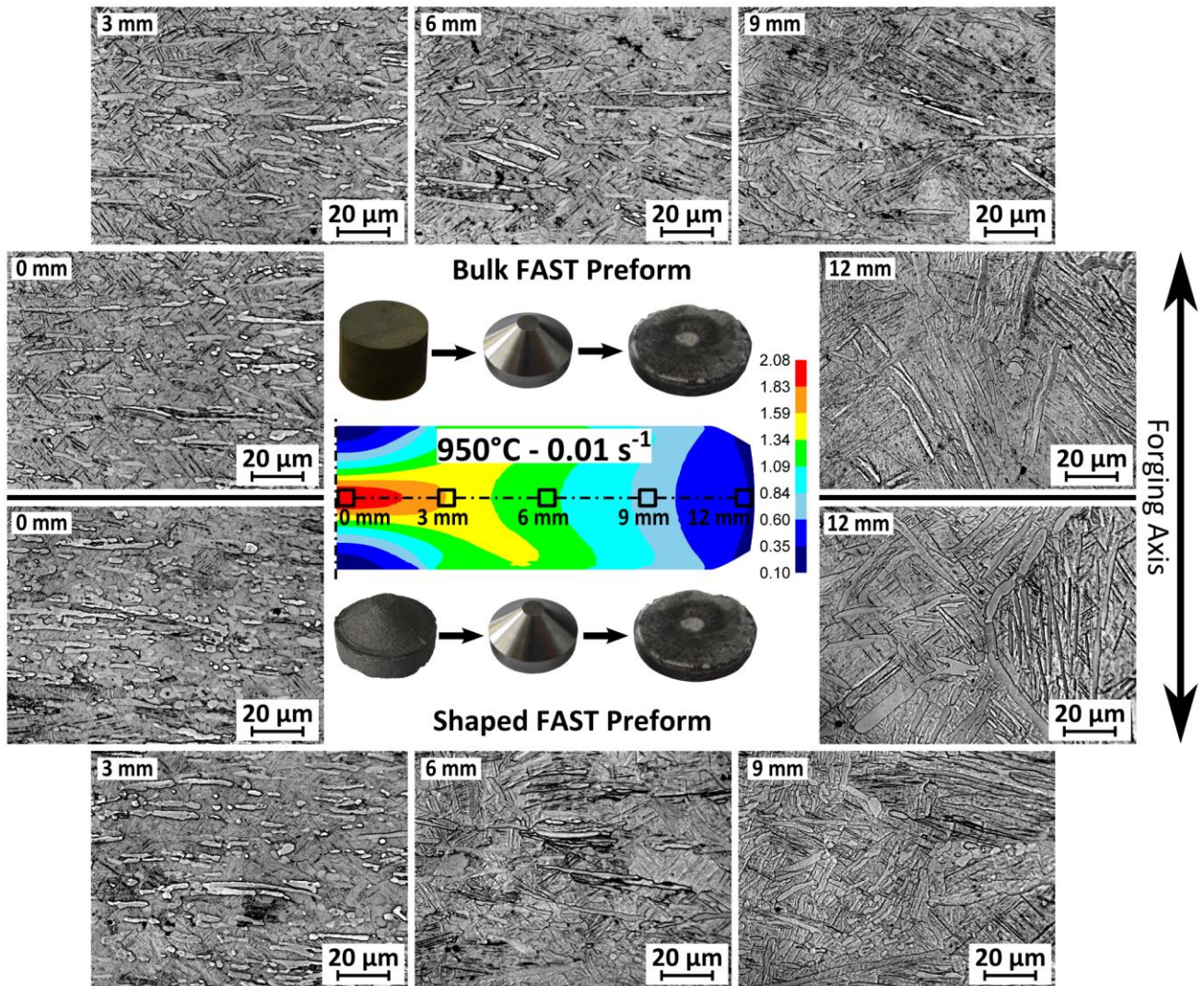
327 testing duplicate samples from the same parent material due to attempting to control the large number of
328 variables seen during hot working of metals. Frictional variations were limited by using similar quantities of
329 lubricant for each test and cleaning the tool posts between tests, but small differences would still occur. The
330 strain rate was closely controlled by the testing software and whilst small oscillations around the set value
331 occurred these were the same for every test and it is thought not large enough to cause the variations in
332 load seen. Due to less than perfect control of the heating in the FTTU causing small oscillations around the
333 target test temperature, typically $\pm 5^\circ\text{C}$, there was some variation in the initial temperature between
334 samples, which would also have a small effect on the loads required.



335
336 *Fig. 10: Graphs of load-displacement curves during hot upset forging of Ti-6Al-4V double truncated cone*
337 *specimens at 950°C and strain rates of 0.01 s⁻¹, 0.1 s⁻¹, and 1 s⁻¹. Bulk (solid lines) and shaped (dashed lines).*

338 3.3 Microstructure Evolution Post One-Step Forging

339 The microstructural evolution for both bulk and shaped double cone specimens under hot uniaxial
340 compression at 950°C, for strain rate regimes of 0.01 s⁻¹, 0.1 s⁻¹ and 1 s⁻¹ is shown in Fig. 11a-11c respectively.
341 The location of the light micrograph images, 3 mm apart along the specimen centreline, is also marked on
342 the FE simulation generated strain profile.

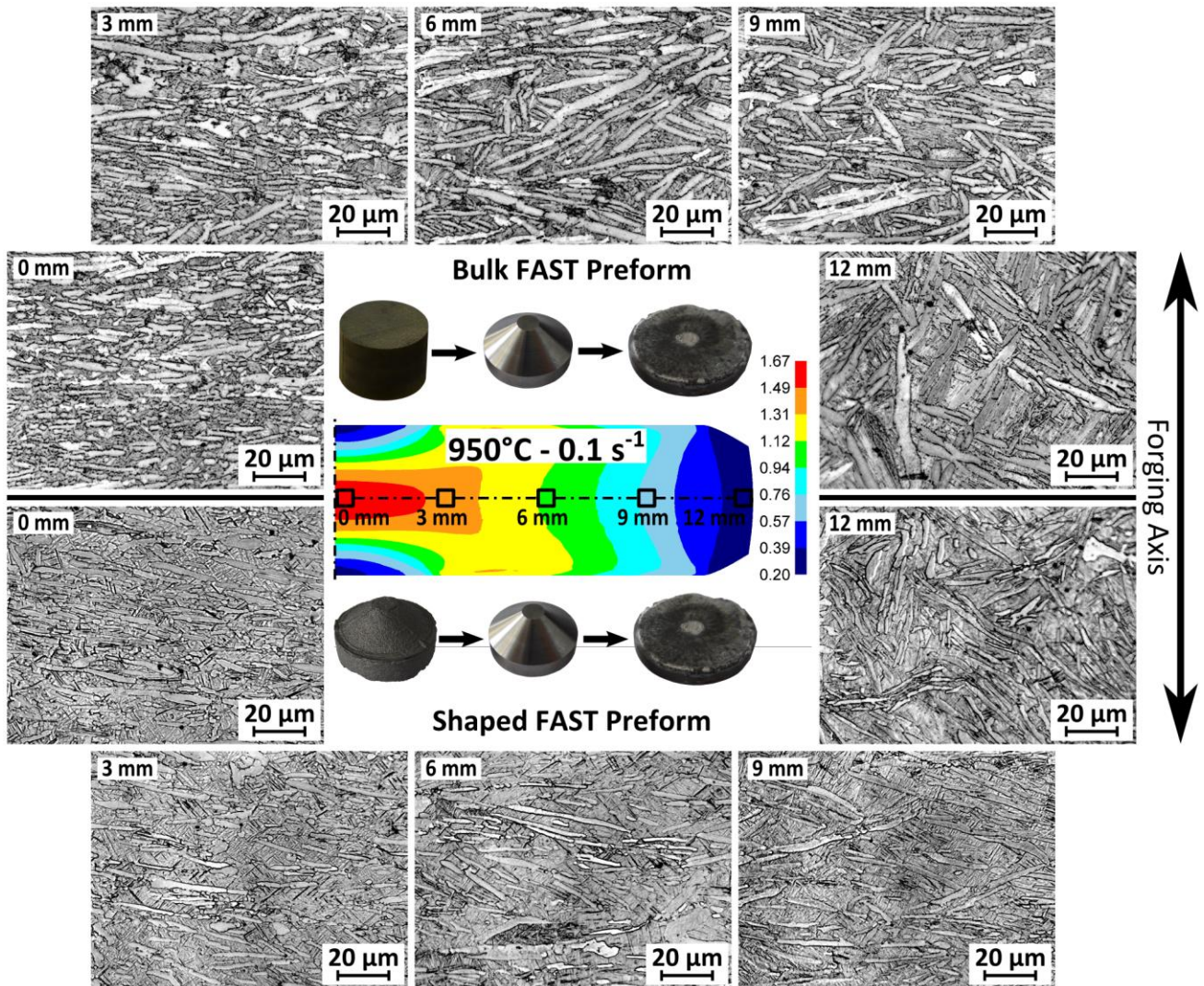


343

344 *Fig. 11a: Light micrographs of the microstructural evolution with increasing strain from edge to centre of the*
 345 *double truncated cone specimens after forging at 950°C and 0.01 s⁻¹; produced from bulk (top) and via*
 346 *shaped FAST (bottom).*

347 At low strains, 12 mm from the centre, there is slight coarsening of the primary α and the transformed β
 348 grains manifest a finer secondary α lath structure than post-FAST due to the water quench and higher
 349 cooling rate. As strain increases, moving towards the specimen centre, it can be seen across both bulk and
 350 shaped double cone specimens at all strain rates that primary α platelets rotate and tend to align
 351 perpendicular to the forging axis; all primary α appears to be fully aligned 6 mm from the centre (a strain of
 352 ~ 1.1). At higher strains break-up of the α platelets into approximately 1-5 μm spheroidal α particles is

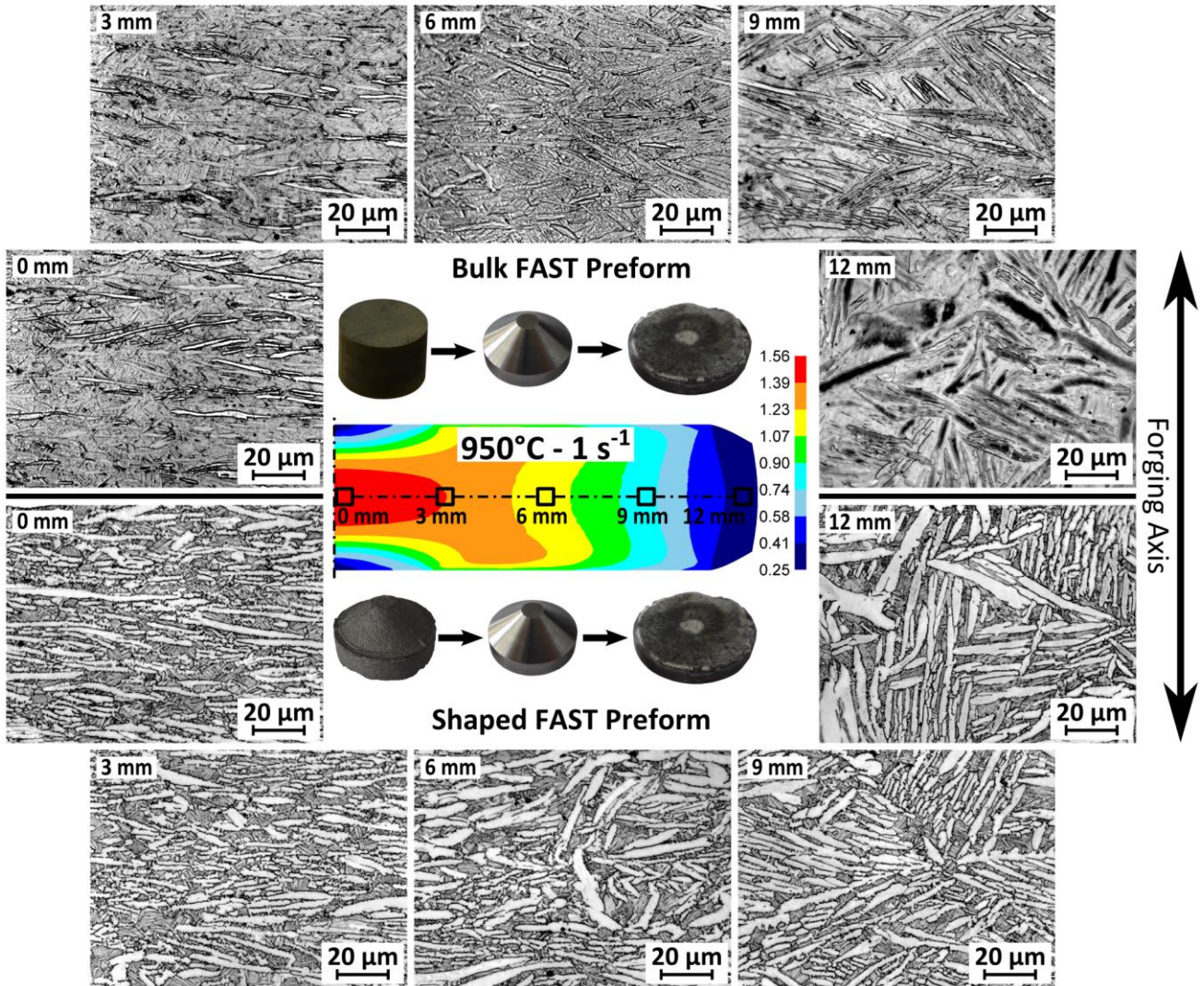
353 observed. As strain rate increases the time for diffusion dominated globurisation of primary α platelets
 354 decreases and it can be seen the amount of spheroidal α particles decreases from Fig. 11a-11c.



355
 356 *Fig. 11b: Light micrographs of the microstructural evolution with increasing strain from edge to centre of the*
 357 *double truncated cone specimens after forging at 950°C and 0.1 s⁻¹; produced from bulk (top) and via shaped*
 358 *FAST (bottom).*

359 The microstructural evolution of shaped double cone specimens compared to double cone specimens
 360 machined from bulk is similar for all strain rates and strains. There has been a significant coarsening of the
 361 primary α in both the bulk double cone specimen at 0.1 s⁻¹ and the shaped double cone specimen at 1 s⁻¹.
 362 This is due to these specimens failing to remain in the robot gripper arms upon retrieval from the test
 363 furnace so that the quenching did not occur automatically and a slower initial cool was experienced; the

364 specimens were manually quenched to room temperature approximately 60-120 s after forging. This slower
 365 cooling rate somewhat hinders a direct comparison between the two specimen types; however, the same
 366 microstructural trends are observed. The observed microstructural evolution is comparable to that reported
 367 during the hot working of conventionally produced Ti-6Al-4V with a colony α microstructure, as reported by
 368 (Semiatin et al., 1999).

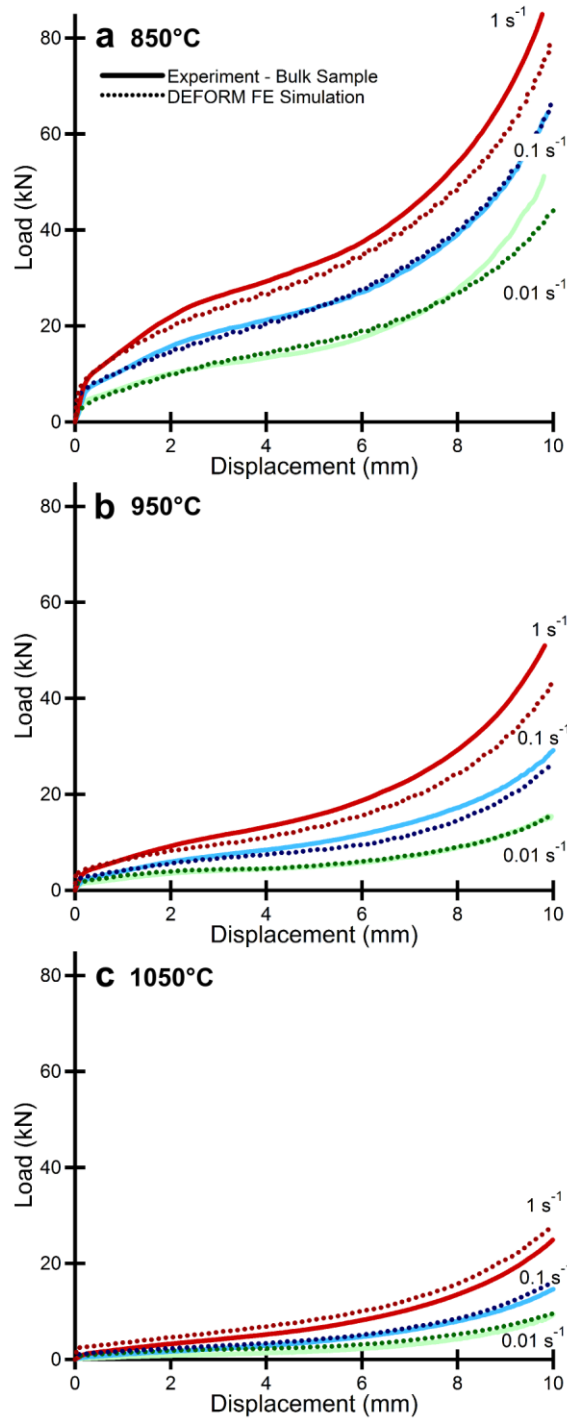


369
 370 *Fig. 11c: Light micrographs of the microstructural evolution with increasing strain from edge to centre of the*
 371 *double truncated cone specimens after forging at 950°C and 1 s⁻¹; produced from bulk (top) and via shaped*
 372 *FAST (bottom).*

373

374 3.4 Finite Element Simulation

375 The load upon the upper tool with respect to its stroke (displacement) was extracted from the data
376 produced by running FE simulations of each experimental point in the test matrix. This data is plotted against
377 the experimentally recorded values of load and displacement for the bulk double cone specimens in Fig. 12.
378 Only data for the bulk double cone specimens is shown to allow clearer comparison, as it has been shown
379 that the shaped double cone specimens produced very similar load data. Overall there is good visual
380 agreement between experimental and predicted values, which gives confidence that the predicted strain
381 profiles are accurate. However, there is slight under prediction at 850°C and 950°C, but slight over prediction
382 at 1050°C. The simulation was set up to mirror the recorded temperature profiles of the experiment, which
383 due to adiabatic heating were not fully isothermal, therefore load changes due to temperature variability
384 were accounted for. However, the material model used was discrete tabulated data (at temperatures of
385 850°C, 950°C, and 1050°C and strain rates of 0.01 s⁻¹, 0.1 s⁻¹, and 1 s⁻¹) with linear interpolation between
386 conditions, which may not be realistic. A constant shear friction factor (\bar{m}) of 0.3 was used and appears to
387 give good visual agreement with experimental conditions, using boron nitride as a release agent, as the end
388 shape of the simulated curves largely matches the experimental even if the absolute values differ. Friction
389 only has a large effect at higher displacements where the contact area has increased; it can be seen in the
390 850°C at 0.01 s⁻¹ curve that a good match is achieved early in the test but the curves diverge at the end,
391 which suggests that this test occurred under increased friction conditions. The material used to produce the
392 data for the FE model was Ti-6Al-4V HDH powder processed in an 80 mm mould with a similar FAST cycle to
393 this work, except a lower pressure of 21 MPa and allowed to free cool; the cooling rate was intermediate to
394 those demonstrated in Fig. 8 and produced a transformed β microstructure with α laths of intermediate
395 thickness to those shown here. This difference in starting microstructure may also explain some of the
396 disparities between simulation and experiment. It should be noted that as tabulated data has been used the
397 FE model can only be employed with confidence within the processing window defined by the extremes of
398 the experimental conditions.



399

400

401

402

403

404

Fig. 12: Graphs comparing the load-displacement curves during the upset forging of double truncated cone specimens at 850°C (a), 950°C (b) and 1050°C (c) at strain rates of 0.01 s⁻¹, 0.1 s⁻¹ and 1 s⁻¹ (as labelled); from bulk FAST material (solid lines) against those obtained from DEFORMTM FE simulation (dotted lines).

405 4. Conclusions

- 406 • This paper has demonstrated at the laboratory scale that it is possible to produce a fully dense and
407 microstructurally refined forged titanium alloy specimen in only two steps from powder. In the
408 long-term the authors believe that this proposed cost-effective hybrid processing route, termed
409 *FAST-forge*, combined with a lower-cost powder from an alternative extraction method will be disruptive
410 technology that will enable a step-change in the economics of titanium alloys.
- 411 • Directly producing shaped FAST double cone specimens did not negatively affect microstructural or
412 deformational behaviour when compared to double cone specimens machined from homogeneous bulk
413 material. There is very good visual correlation between the two types of specimens. This establishes that
414 using FAST to produce shaped preforms has the potential to be an effective intermediate step in the
415 *FAST-forge* process. Further work is required to explore the possibilities and limitations of the
416 technology prior to scale-up, but in future it should be possible to accurately produce shaped FAST
417 preforms for a variety of final components.
- 418 • At the current level of FAST technology commercially available the cost-effectiveness achieved by the
419 *FAST-forge* processing route will vary from component to component; an economic assessment on case
420 by case basis would be required. The initial set-up costs may negate benefits for small batch production
421 and speed of processing limitations may exclude products requiring continuous or very large/quick batch
422 production. However, with expensive feedstocks such as titanium there may still be cost reductions to
423 be found via *FAST-forge*. The tooling costs for FAST compare favourably against HIP, where the steel can
424 bond to the titanium and needs to be machined away, as the majority of the graphite mould assembly
425 is reusable. The longevity and cost-effectiveness of the mould assembly in terms of both material and
426 geometry needs to be investigated further to give an understanding of tooling costs as the technology
427 progresses in size and part complexity.

- 428 • The response of Ti-6Al-4V FAST material under forging conditions is very similar to that seen when
429 thermomechanically working conventional Ti-6Al-4V billet material; post-sintering FAST preforms have
430 characteristics similar to conventional melt, multi-step forged product.
- 431 • The agreement between experimental load-displacement data and FE simulation data gives confidence
432 that the material model utilised can be used to model the forging of more complex geometries as the
433 FAST-*forge* process develops.
- 434 • Initial examination of the microstructural evolution indicates the level of strain, temperature and strain
435 rate required to break up the post FAST microstructure and achieve a bimodal α - β microstructure, but
436 further analysis is needed to tie key microstructural features to thermomechanical processing
437 parameters for use in a simple microstructural prediction model.
- 438 • It is further anticipated that if the required mechanical properties of a component are identified then a
439 microstructure necessary to meet these can be predicted. Using FE simulation, linked to a
440 microstructural model, the shape of the preform could be iteratively optimised so that the one-step
441 precision forging operation can produce the correct levels of strain at the forging conditions to yield the
442 appropriate microstructure to meet the property requirements.

443

444 **Acknowledgements**

445 The authors acknowledge the Engineering and Physical Sciences Research Council's Advanced Metallic
446 Systems Centre for Doctoral Training for funding N. S. Weston (Grant Number EP/G036950/1). Thanks go to
447 the Defence Science and Technology Laboratory for additional funding, and specifically Dr Matthew Lunt for
448 his support. The authors also recognise Dr Fatos Derguti for technical discussions and Dr Adam Tudball of
449 Kennametal Manufacturing (UK) Ltd. for technical knowledge and assistance when using their large-scale
450 FAST furnace.

451

452 **Appendix**

453 **TABLE 1:** Tabulated flow stress data at the indicated testing conditions and strain levels that was
 454 used as the material model for FE modelling of the forging of Ti-6Al-4V HDH powder consolidated using
 455 FAST at a heating rate of 100°Cmin⁻¹ with dwell conditions of 1200°C and 50 MPa held for 30 minutes.

Strain	Test Conditions								
	850°C			950°C			1050°C		
	0.01 s ⁻¹	0.1 s ⁻¹	1 s ⁻¹	0.01 s ⁻¹	0.1 s ⁻¹	1 s ⁻¹	0.01 s ⁻¹	0.1 s ⁻¹	1 s ⁻¹
0.000	0.0	0.0	0.0	0.0	0.0	0.0	0.0	0.0	0.0
0.010	31.3	98.4	94.0	24.7	50.3	39.6	7.2	20.0	43.3
0.015	57.7	146.3	149.1	30.6	58.0	57.6	8.8	28.1	44.0
0.020	90.5	175.6	188.2	32.1	60.5	72.4	10.0	31.5	45.0
0.030	111.5	192.0	213.4	34.0	60.2	75.5	10.6	32.6	46.3
0.050	114.9	192.3	220.4	34.3	59.3	78.5	11.5	33.4	47.4
0.100	114.5	188.0	225.4	34.8	58.4	82.9	12.4	34.1	48.6
0.150	112.5	183.7	227.5	34.6	57.4	87.3	13.2	34.4	49.7
0.200	110.0	178.1	229.6	33.6	56.3	89.5	14.1	34.1	50.8
0.250	106.9	172.8	231.5	33.0	54.8	89.8	14.9	33.7	51.9
0.300	105.1	168.1	228.1	32.4	53.8	89.9	15.8	33.2	53.0
0.400	98.8	160.0	218.5	31.5	51.9	88.7	16.3	32.2	53.3
0.500	95.6	153.7	208.5	30.6	50.7	87.6	16.8	31.2	53.0
0.600	92.6	147.8	202.1	30.1	50.5	87.2	16.2	30.8	53.1
0.700	89.1	143.4	195.4	29.7	50.2	87.2	15.3	30.3	53.1
0.800	84.1	138.4	189.8	29.3	50.2	87.2	14.9	30.2	53.1
0.900	82.1	135.6	187.8	29.0	50.2	87.2	14.2	30.2	53.1
1.000	79.3	135.2	186.6	28.6	50.2	87.2	13.8	30.2	53.1
1.200	73.8	135.2	186.6	28.2	50.2	87.2	12.8	30.2	53.1
5.000	73.8	135.2	186.6	28.2	50.2	87.2	11.5	30.2	53.1

456

457 **References**

458 Armstrong, D.R., Borys, S.S., Anderson, R.P., 1999. Method of making metals and other elements from the
 459 halid vapor of the metal. US5958106 A.

460 Benson, L.L., Mellor, I., Jackson, M., 2016. Direct reduction of synthetic rutile using the FFC process to
 461 produce low-cost novel titanium alloys. *J. Mater. Sci.* 51, 1–12. doi:10.1007/s10853-015-9718-1

462 Doblin, C., Chryss, A., Monch, A., 2012. Titanium powder from the TiRO™ process. *Key Eng. Mater.* 520, 95–
 463 100. doi:10.4028/www.scientific.net/KEM.520.95

464 Duz, V.A., Matviychuk, M., Klevtsov, A., Moxson, V., 2016. Industrial application of titanium hydride powder.
 465 *Met. Powder Rep.* doi:10.1016/j.mprp.2016.02.051

466 Fray, D.J., 2008. Novel methods for the production of titanium. *Int. Mater. Rev.* 53, 317–325.
 467 doi:10.1179/174328008X324594

468 Frei, J.M., Anselmi-Tamburini, U., Munir, Z.A., 2007. Current effects on neck growth in the sintering of
 469 copper spheres to copper plates by the pulsed electric current method. *J. Appl. Phys.* 101, 114914-1-
 470 114914–8. doi:10.1063/1.2743885

471 German, R.M., 2014. *Sintering: From Empirical Observations to Scientific Principles*, Elsevier Inc.
 472 doi:10.1016/B978-0-12-401682-8.00011-2

473 Hulbert, D.M., Anders, A., Dudina, D. V., Andersson, J., Jiang, D., Unuvar, C., Anselmi-Tamburini, U., Lavernia,
 474 E.J., Mukherjee, A.K., 2008. The absence of plasma in “spark plasma sintering.” *J. Appl. Phys.* 104,
 475 33305. doi:10.1063/1.2963701

476 Jackson, M., Dashwood, R.J., Christodoulou, L., Flower, H.M., 2000. Application of novel technique to

- 477 examine thermomechanical processing of near β alloy Ti–10V–2Fe–3Al. *Mater. Sci. Technol.* 16, 1437–
 478 1444. doi:10.1179/026708300101507433
- 479 Joshi, V.A., 2006. *Titanium Alloys: An Atlas of Structures and Fracture Features*, 1st ed. CRC Press Taylor &
 480 Francis Group, LLC.
- 481 Kim, Y., Kim, E.-P., Song, Y.-B., Lee, S.H., Kwon, Y.-S., 2014. Microstructure and mechanical properties of hot
 482 isostatically pressed Ti–6Al–4V alloy. *J. Alloys Compd.* 603, 207–212. doi:10.1016/j.jallcom.2014.03.022
- 483 Kraft, E.H., 2004. Summary of emerging titanium cost reduction technologies, A Study Performed For US
 484 Department of Energy And Oak Ridge National Laboratory Subcontract 4000023694. Vancouver WA.
- 485 Lütjering, G., 1998. Influence of processing on microstructure and mechanical properties of (α + β) titanium
 486 alloys. *Mater. Sci. Eng. A* 243, 32–45. doi:10.1016/S0921-5093(97)00778-8
- 487 Mellor, I., Grainger, L., Rao, K., Deane, J., Conti, M., Doughty, G., Vaughan, D., 2015. Titanium Powder
 488 Production via the Metalysis Process, in: Qian, M., Froes, F.H. (Eds.), *Titanium Powder Metallurgy: Science, Technology and Applications*. Butterworth-Heinemann Ltd, Oxford, UK, pp. 51–67.
 489 doi:10.1016/B978-0-12-800054-0.00004-6
- 490 Munir, Z.A., Quach, D. V., Ohyanagi, M., 2011. Electric current activation of sintering: A review of the pulsed
 491 electric current sintering process. *J. Am. Ceram. Soc.* 94, 1–19. doi:10.1111/j.1551-2916.2010.04210.x
- 492 Musa, C., Licheri, R., Locci, A.M., Orrù, R., Cao, G., Rodriguez, M.A., Jaworska, L., 2009. Energy efficiency
 493 during conventional and novel sintering processes: the case of Ti–Al₂O₃–TiC composites. *J. Clean. Prod.*
 494 17, 877–882. doi:10.1016/j.jclepro.2009.01.012
- 495 Orrù, R., Licheri, R., Locci, A.M., Cincotti, A., Cao, G., 2009. Consolidation/synthesis of materials by electric
 496 current activated/assisted sintering. *Mater. Sci. Eng. R* 63, 127–287. doi:10.1016/j.mser.2008.09.003
- 497 Rasband, W.S., 1997. ImageJ, ImageJ. U.S National Institutes of Health, Bethesda, Maryland, USA,
 498 <http://imagej.nih.gov/ij/>.
- 499 Scientific Forming Technologies Corporation, 2016. DEFORM™ (v.11.0.1), DEFORM 11.0.1. SFTC, Columbus,
 500 Ohio.
- 501 Semiatin, S., Seetharaman, V., Weiss, I., 1999. Flow behavior and globularization kinetics during hot working
 502 of Ti–6Al–4V with a colony alpha microstructure. *Mater. Sci. Eng. A* 263, 257–271. doi:10.1016/S0921-
 503 5093(98)01156-3
- 504 Van Vuuren, D.S., Oosthuizen, S.J., Heydenrych, M.D., 2011. Titanium production via metallothermic
 505 reduction of TiCl₄ in molten salt: Problems and products. *J. South. African Inst. Min. Metall.* 111, 141–
 506 148.
- 507 Weston, N.S., Derguti, F., Tudball, A., Jackson, M., 2015. Spark plasma sintering of commercial and
 508 development titanium alloy powders. *J. Mater. Sci.* 50, 4860–4878. doi:10.1007/s10853-015-9029-6
- 509 Withers, J.C., 2015. Production of Titanium Powder by an Electrolytic Method and Compaction of the
 510 Powder, in: Qian, M., Froes, F.H. (Eds.), *Titanium Powder Metallurgy: Science, Technology and Applications*. Butterworth-Heinemann Ltd, Oxford, UK, pp. 33–50. doi:10.1016/B978-0-12-800054-
 511 0.00003-4
- 512 Xu, L., Guo, R., Bai, C., Lei, J., Yang, R., 2014. Effect of Hot Isostatic Pressing Conditions and Cooling Rate on
 513 Microstructure and Properties of Ti-6Al-4V Alloy from Atomized Powder. *J. Mater. Sci. Technol.* 30,
 514 1289–1295. doi:10.1016/j.jmst.2014.04.011

517
 518 TABLE 1: Tabulated flow stress data at the indicated testing conditions and strain levels that was
 519 used as the material model for FE modelling of the forging of Ti-6Al-4V HDH powder consolidated using
 520 FAST at a heating rate of 100°Cmin⁻¹ with dwell conditions of 1200°C and 50 MPa held for 30 minutes.

521 *Fig. 1: Chart demonstrating the two main areas of production costs for 25 mm titanium alloy plate when*
 522 *conventionally processed; with relative cost factors for each sub-area also shown. Produced from data*
 523 *reported in (Kraft, 2004).*

524 Fig. 2: Schematic diagram outlining the two-step hybrid “FAST-forge” process – a proposed cost-effective
525 solid-state processing route for producing titanium alloy components from powder.

526 Fig. 3: Photograph demonstrating the outcome at each stage of the two-step FAST-forge process; the starting
527 Ti-6Al-4V HDH powder (left) to the intermediate shaped preform billet, a double truncated cone FAST
528 specimen with a light surface machine (centre), and the final forged specimen (right).

529 Fig. 4: Schematic showing the two methods used to make the double truncated cone specimens. Method 1
530 produced a 100 mm diameter x 15 mm thick FAST disc, which smaller cylinders were extracted from via
531 electro-discharge machining (EDM), and then machined to the final dimensions shown (known as “bulk”
532 double cone specimens). Method 2 used shaped graphite inserts in a 20 mm diameter FAST mould assembly
533 to produce shaped preforms, which then had a surface machine to give the final dimensions shown (known as
534 “shaped” double cone specimens).

535 Fig. 5: Light micrographs of the Ti-6Al-4V HDH powder’s particle morphology after etching with Kroll’s
536 reagent (a) and microstructure under cross-polarised light (b).

537 Fig. 6: Photograph of the FCT Systeme GmbH Type HP D 25 FAST Furnace at The University of Sheffield (right);
538 showing detail of the graphite mould assembly held between the conducting hydraulic rams (inset right).
539 Schematic cross-section showing the main components of the FAST system and mould assembly used (bottom
540 left) and a graph outlining the variation in major processing parameters during a typical FAST cycle (top left).

541 Fig. 7: Photographs outlining the major components of The University of Sheffield’s thermomechanical
542 compression machine (a), close-up view of the tool posts and furnace (b) (note the furnace has been moved
543 to the rear to enable viewing of the tool posts), close-up of a double truncated cone specimen held in the
544 robot gripper arms (c).

545 Fig. 8: Graph showing the temperature profiles during FAST processing of three types of Ti-6Al-4V specimen
546 (a). A 100 mm diameter disc used for bulk double cone specimens; allowed to “free” cool after current switch-
547 off (solid line). A 20 mm shaped mould when allowed to “free” cool after current switch-off (dotted line) with
548 associated microstructure (b). A 20 mm shaped mould with “controlled” cool (dashed line) and associated
549 microstructure (c).

550 Fig. 9: Micrographs of Ti-6Al-4V double truncated cone specimens produced via FAST at a dwell temperature
551 of 1200°C. Showing microstructures from a shaped specimen (Shaped 1-4) at the locations outlined in the top
552 left diagram; and a characteristic microstructure of the homogeneous bulk specimen (bottom right).

553 Fig. 10: Graphs of load-displacement curves during hot upset forging of Ti-6Al-4V double truncated cone
554 specimens at 950°C and strain rates of 0.01 s⁻¹, 0.1 s⁻¹, and 1 s⁻¹. Bulk (solid lines) and shaped (dashed lines).

555 *Fig. 11a: Light micrographs of the microstructural evolution with increasing strain from edge to centre of the*
556 *double truncated cone specimens after forging at 950°C and 0.01 s⁻¹; produced from bulk (top) and via*
557 *shaped FAST (bottom).*

558 *Fig. 11b: Light micrographs of the microstructural evolution with increasing strain from edge to centre of the*
559 *double truncated cone specimens after forging at 950°C and 0.1 s⁻¹; produced from bulk (top) and via shaped*
560 *FAST (bottom).*

561 *Fig. 11c: Light micrographs of the microstructural evolution with increasing strain from edge to centre of the*
562 *double truncated cone specimens after forging at 950°C and 1 s⁻¹; produced from bulk (top) and via shaped*
563 *FAST (bottom).*

564 *Fig. 12: Graphs comparing the load-displacement curves during the upset forging of double truncated cone*
565 *specimens at 850°C (a), 950°C (b) and 1050°C (c) at strain rates of 0.01 s⁻¹, 0.1 s⁻¹ and 1 s⁻¹ (as labelled); from*
566 *bulk FAST material (solid lines) against those obtained from DEFORMTM FE simulation (dotted lines).*